

Neutral kaon interferometry in Au+Au collisions at $\sqrt{s_{NN}} = 200$ GeV

B. I. Abelev,⁵⁰ M. M. Aggarwal,³⁰ Z. Ahammed,⁴⁵ J. Amonett,²⁰ B. D. Anderson,²⁰ M. Anderson,⁶ D. Arkhipkin,¹³ G. S. Averichev,¹² Y. Bai,²⁸ J. Balewski,¹⁷ O. Barannikova,⁹ L. S. Barnby,² J. Baudot,¹⁸ S. Bekele,²⁹ V. V. Belaga,¹² A. Bellingeri-Laurikainen,⁴⁰ R. Bellwied,⁴⁸ F. Benedosso,²⁸ S. Bhardwaj,³⁵ A. Bhasin,¹⁹ A. K. Bhati,³⁰ H. Bichsel,⁴⁷ J. Bielcik,⁵⁰ J. Bielcikova,⁵⁰ L. C. Bland,³ S.-L. Blyth,²² B. E. Bonner,³⁶ M. Botje,²⁸ J. Bouchet,⁴⁰ A. V. Brandin,²⁶ A. Bravar,³ T. P. Burton,² M. Bystersky,¹¹ R. V. Cadman,¹ X. Z. Cai,³⁹ H. Caines,⁵⁰ M. Calderón de la Barca Sánchez,⁶ J. Castillo,²⁸ O. Catu,⁵⁰ D. Cebra,⁶ Z. Chajecki,²⁹ P. Chaloupka,¹¹ S. Chattopadhyay,⁴⁵ H. F. Chen,³⁸ J. H. Chen,³⁹ J. Cheng,⁴³ M. Cherney,¹⁰ A. Chikanian,⁵⁰ W. Christie,³ J. P. Coffin,¹⁸ T. M. Cormier,⁴⁸ M. R. Cosentino,³⁷ J. G. Cramer,⁴⁷ H. J. Crawford,⁵ D. Das,⁴⁵ S. Das,⁴⁵ S. Dash,¹⁵ M. Daugherty,⁴² M. M. de Moura,³⁷ T. G. Dedovich,¹² M. DePhillips,³ A. A. Derevschikov,³² L. Didenko,³ T. Dietel,¹⁴ P. Djawotho,¹⁷ S. M. Dogra,¹⁹ W. J. Dong,⁷ X. Dong,³⁸ J. E. Draper,⁶ F. Du,⁵⁰ V. B. Dunin,¹² J. C. Dunlop,³ M. R. Dutta Mazumdar,⁴⁵ V. Eckardt,²⁴ W. R. Edwards,²² L. G. Efimov,¹² V. Emelianov,²⁶ J. Engelage,⁵ G. Eppley,³⁶ B. Erasmus,⁴⁰ M. Estienne,¹⁸ P. Fachini,³ R. Fatemi,²³ J. Fedorisin,¹² K. Filimonov,²² P. Filip,¹³ E. Finch,⁵⁰ V. Fine,³ Y. Fisyak,³ J. Fu,⁴⁹ C. A. Gagliardi,⁴¹ L. Gaillard,² M. S. Ganti,⁴⁵ V. Ghazikhanian,⁷ P. Ghosh,⁴⁵ J. E. Gonzalez,⁷ Y. G. Gorbunov,¹⁰ H. Gos,⁴⁶ O. Grebenyuk,²⁸ D. Grosnick,⁴⁴ S. M. Guertin,⁷ K. S. F. F. Guimaraes,³⁷ N. Gupta,¹⁹ T. D. Gutierrez,⁶ B. Haag,⁶ T. J. Hallman,³ A. Hamed,⁴⁸ J. W. Harris,⁵⁰ W. He,¹⁷ M. Heinz,⁵⁰ T. W. Henry,⁴¹ S. Hepplemann,³¹ B. Hippolyte,¹⁸ A. Hirsch,³³ E. Hjort,²² A. M. Hoffman,²³ G. W. Hoffmann,⁴² M. J. Horner,²² H. Z. Huang,⁷ S. L. Huang,³⁸ E. W. Hughes,⁴ T. J. Humanic,²⁹ G. Igo,⁷ P. Jacobs,²² W. W. Jacobs,¹⁷ P. Jakl,¹¹ F. Jia,²¹ H. Jiang,⁷ P. G. Jones,² E. G. Judd,⁵ S. Kabana,⁴⁰ K. Kang,⁴³ J. Kapitan,¹¹ M. Kaplan,⁸ D. Keane,²⁰ A. Kechechyan,¹² V. Yu. Khodyrev,³² B. C. Kim,³⁴ J. Kiryluk,²³ A. Kisiel,⁴⁶ E. M. Kislov,¹² S. R. Klein,²² A. Kocoloski,²³ D. D. Koetke,⁴⁴ T. Kollegger,¹⁴ M. Kopytine,²⁰ L. Kotchenda,²⁶ V. Kouchpil,¹¹ K. L. Kowalik,²² M. Kramer,²⁷ P. Kravtsov,²⁶ V. I. Kravtsov,³² K. Krueger,¹ C. Kuhn,¹⁸ A. I. Kulikov,¹² A. Kumar,³⁰ A. A. Kuznetsov,¹² M. A. C. Lamont,⁵⁰ J. M. Landgraf,³ S. Lange,¹⁴ S. LaPointe,⁴⁸ F. Laue,³ J. Lauret,³ A. Lebedev,³ R. Lednický,¹³ C.-H. Lee,³⁴ S. Lehocka,¹² M. J. LeVine,³ C. Li,³⁸ Q. Li,⁴⁸ Y. Li,⁴³ G. Lin,⁵⁰ X. Lin,⁴⁹ S. J. Lindenbaum,²⁷ M. A. Lisa,²⁹ F. Liu,⁴⁹ H. Liu,³⁸ J. Liu,³⁶ L. Liu,⁴⁹ Z. Liu,⁴⁹ T. Ljubicic,³ W. J. Llope,³⁶ H. Long,⁷ R. S. Longacre,³ W. A. Love,³ Y. Lu,⁴⁹ T. Ludlam,³ D. Lynn,³ G. L. Ma,³⁹ J. G. Ma,⁷ Y. G. Ma,³⁹ D. Magestro,²⁹ D. P. Mahapatra,¹⁵ R. Majka,⁵⁰ L. K. Mangotra,¹⁹ R. Manweiler,⁴⁴ S. Margetis,²⁰ C. Markert,⁴² L. Martin,⁴⁰ H. S. Matis,²² Yu. A. Matulenko,³² C. J. McClain,¹ T. S. McShane,¹⁰ Yu. Melnick,³² A. Meschanin,³² J. Millane,²³ M. L. Miller,²³ N. G. Minaev,³² S. Mioduszewski,⁴¹ C. Mironov,²⁰ A. Mischke,²⁸ D. K. Mishra,¹⁵ J. Mitchell,³⁶ B. Mohanty,⁴⁵ L. Molnar,³³ C. F. Moore,⁴² D. A. Morozov,³² M. G. Munhoz,³⁷ B. K. Nandi,¹⁶ C. Nattrass,⁵⁰ T. K. Nayak,⁴⁵ J. M. Nelson,² P. K. Netrakanti,⁴⁵ L. V. Nogach,³² S. B. Nurushev,³² G. Odyniec,²² A. Ogawa,³ V. Okorokov,²⁶ M. Oldenburg,²² D. Olson,²² M. Pachr,¹¹ S. K. Pal,⁴⁵ Y. Panebratsev,¹² S. Y. Panitkin,³ A. I. Pavlinov,⁴⁸ T. Pawlak,⁴⁶ T. Peitzmann,²⁸ V. Perevoztchikov,³ C. Perkins,⁵ W. Peryt,⁴⁶ S. C. Phatak,¹⁵ R. Picha,⁶ M. Planinic,⁵¹ J. Pluta,⁴⁶ N. Poljak,⁵¹ N. Porile,³³ J. Porter,⁴⁷ A. M. Poskanzer,²² M. Potekhin,³ E. Potrebenikova,¹² B. V. K. S. Potukuchi,¹⁹ D. Prindle,⁴⁷ C. Pruneau,⁴⁸ J. Putschke,²² G. Rakness,³¹ R. Raniwala,³⁵ S. Raniwala,³⁵ R. L. Ray,⁴² S. V. Razin,¹² J. Reinnarth,⁴⁰ D. Relyea,⁴ F. Retiere,²² A. Ridiger,²⁶ H. G. Ritter,²² J. B. Roberts,³⁶ O. V. Rogachevskiy,¹² J. L. Romero,⁶ A. Rose,²² C. Roy,⁴⁰ L. Ruan,²² M. J. Russcher,²⁸ R. Sahoo,¹⁵ T. Sakuma,²³ S. Salur,⁵⁰ J. Sandweiss,⁵⁰ M. Sarsour,⁴¹ P. S. Sazhin,¹² J. Schambach,⁴² R. P. Scharenberg,³³ N. Schmitz,²⁴ K. Schweda,²² J. Seger,¹⁰ I. Selyuzhenkov,⁴⁸ P. Seyboth,²⁴ A. Shabetai,²⁰ E. Shahaliev,¹² M. Shao,³⁸ M. Sharma,³⁰ W. Q. Shen,³⁹ S. S. Shimanskiy,¹² E. P. Sichtermann,²² F. Simon,²³ R. N. Singaraju,⁴⁵ N. Smirnov,⁵⁰ R. Snellings,²⁸ G. Sood,⁴⁴ P. Sorensen,³ J. Sowinski,¹⁷ J. Speltz,¹⁸ H. M. Spinka,¹ B. Srivastava,³³ A. Stadnik,¹² T. D. S. Stanislaus,⁴⁴ R. Stock,¹⁴ A. Stolpovsky,⁴⁸ M. Strikhanov,²⁶ B. Stringfellow,³³ A. A. P. Suaide,³⁷ E. Sugarbaker,²⁹ M. Sumera,¹¹ Z. Sun,²¹ B. Surrow,²³ M. Swanger,¹⁰ T. J. M. Symons,²² A. Szanto de Toledo,³⁷ A. Tai,⁷ J. Takahashi,³⁷ A. H. Tang,³ T. Tarnowsky,³³ D. Thein,⁷ J. H. Thomas,²² A. R. Timmins,² S. Timoshenko,²⁶ M. Tokarev,¹² T. A. Trainor,⁴⁷ S. Trentalange,⁷ R. E. Tribble,⁴¹ O. D. Tsai,⁷ J. Ulyery,³³ T. Ullrich,³ D. G. Underwood,¹ G. Van Buren,³ N. van der Kolk,²⁸ M. van Leeuwen,²² A. M. Vander Molen,²⁵ R. Varma,¹⁶ I. M. Vasilevski,¹³ A. N. Vasiliev,³² R. Vernet,¹⁸ S. E. Vigdor,¹⁷ Y. P. Viyogi,¹⁵ S. Vokal,¹² S. A. Voloshin,⁴⁸ W. T. Waggner,¹⁰ F. Wang,³³ G. Wang,⁷ J. S. Wang,²¹ X. L. Wang,³⁸ Y. Wang,⁴³ J. W. Watson,²⁰ J. C. Webb,⁴⁴ G. D. Westfall,²⁵ A. Wetzler,²² C. Whitten Jr.,⁷ H. Wieman,²² S. W. Wissink,¹⁷ R. Witt,⁵⁰ J. Wood,⁷ J. Wu,³⁸ N. Xu,²² Q. H. Xu,²² Z. Xu,³ P. Yepes,³⁶ I.-K. Yoo,³⁴ V. I. Yurevich,¹² W. Zhan,²¹ H. Zhang,³ W. M. Zhang,²⁰ Y. Zhang,³⁸ Z. P. Zhang,³⁸ Y. Zhao,³⁸ C. Zhong,³⁹ R. Zoukarneev,¹³ Y. Zoukarneeva,¹³ A. N. Zubarev,¹² and J. X. Zuo³⁹

(STAR Collaboration)

¹Argonne National Laboratory, Argonne, Illinois 60439, USA²University of Birmingham, Birmingham, United Kingdom³Brookhaven National Laboratory, Upton, New York 11973, USA⁴California Institute of Technology, Pasadena, California 91125, USA⁵University of California, Berkeley, California 94720, USA⁶University of California, Davis, California 95616, USA⁷University of California, Los Angeles, California 90095, USA⁸Carnegie Mellon University, Pittsburgh, Pennsylvania 15213, USA⁹University of Illinois at Chicago, Chicago, Illinois, USA¹⁰Creighton University, Omaha, Nebraska 68178, USA

- ¹¹*Nuclear Physics Institute AS CR, 250 68 Řež/Prague, Czech Republic*
¹²*Laboratory for High Energy (JINR), Dubna, Russia*
¹³*Particle Physics Laboratory (JINR), Dubna, Russia*
¹⁴*University of Frankfurt, Frankfurt, Germany*
¹⁵*Institute of Physics, Bhubaneswar 751005, India*
¹⁶*Indian Institute of Technology, Mumbai, India*
¹⁷*Indiana University, Bloomington, Indiana 47408, USA*
¹⁸*Institut de Recherches Subatomiques, Strasbourg, France*
¹⁹*University of Jammu, Jammu 180001, India*
²⁰*Kent State University, Kent, Ohio 44242, USA*
²¹*Institute of Modern Physics, Lanzhou, People's Republic of China*
²²*Lawrence Berkeley National Laboratory, Berkeley, California 94720, USA*
²³*Massachusetts Institute of Technology, Cambridge, Massachusetts, 02139-4307, USA*
²⁴*Max-Planck-Institut für Physik, Munich, Germany*
²⁵*Michigan State University, East Lansing, Michigan 48824, USA*
²⁶*Moscow Engineering Physics Institute, Moscow, Russia*
²⁷*City College of New York, New York City, New York 10031, USA*
²⁸*NIKHEF and Utrecht University, Amsterdam, The Netherlands*
²⁹*Ohio State University, Columbus, Ohio 43210, USA*
³⁰*Panjab University, Chandigarh 160014, India*
³¹*Pennsylvania State University, University Park, Pennsylvania 16802, USA*
³²*Institute of High Energy Physics, Protvino, Russia*
³³*Purdue University, West Lafayette, Indiana 47907, USA*
³⁴*Pusan National University, Pusan, Republic of Korea*
³⁵*University of Rajasthan, Jaipur 302004, India*
³⁶*Rice University, Houston, Texas 77251, USA*
³⁷*Universidade de Sao Paulo, Sao Paulo, Brazil*
³⁸*University of Science & Technology of China, Hefei 230026, People's Republic of China*
³⁹*Shanghai Institute of Applied Physics, Shanghai 201800, People's Republic of China*
⁴⁰*SUBATECH, Nantes, France*
⁴¹*Texas A&M University, College Station, Texas 77843, USA*
⁴²*University of Texas, Austin, Texas 78712, USA*
⁴³*Tsinghua University, Beijing 100084, People's Republic of China*
⁴⁴*Valparaiso University, Valparaiso, Indiana 46383, USA*
⁴⁵*Variable Energy Cyclotron Centre, Kolkata 700064, India*
⁴⁶*Warsaw University of Technology, Warsaw, Poland*
⁴⁷*University of Washington, Seattle, Washington 98195, USA*
⁴⁸*Wayne State University, Detroit, Michigan 48201, USA*
⁴⁹*Institute of Particle Physics, CCNU (HZNU), Wuhan 430079, People's Republic of China*
⁵⁰*Yale University, New Haven, Connecticut 06520, USA*
⁵¹*University of Zagreb, Zagreb, HR-10002, Croatia*
- (Received 7 August 2006; published 15 November 2006)

We present the first statistically meaningful results from two- K_s^0 interferometry in heavy-ion collisions at $\sqrt{s_{NN}} = 200$ GeV. A model that takes the effect of the strong interaction into account has been used to fit the measured correlation function. The effects of single and coupled channels were explored. At the mean transverse mass $\langle m_T \rangle = 1.07$ GeV, we obtain the values $R = 4.09 \pm 0.46(\text{stat}) \pm 0.31(\text{sys})$ fm and $\lambda = 0.92 \pm 0.23(\text{stat}) \pm 0.13(\text{sys})$, where R and λ are the invariant radius and chaoticity parameters, respectively. The results are qualitatively consistent with m_T systematics established with pions in a scenario characterized by a strong collective flow.

DOI: [10.1103/PhysRevC.74.054902](https://doi.org/10.1103/PhysRevC.74.054902)

PACS number(s): 25.75.Gz

I. INTRODUCTION

Lattice quantum chromodynamics (QCD) calculations predict that a phase transition from hadronic matter to a new state of matter called a quark gluon plasma (QGP) occurs

at sufficiently large energy densities [1]. Creation and study of such a deconfined state of matter is the primary goal of the heavy-ion collisions program at the Relativistic Heavy Ion Collider (RHIC). A first-order phase transition from the

QGP back to normal hadronic matter is believed to delay the expansion of the hot reaction zone created in the collision [2]. A delayed expansion means a long duration of particle emission, leading to a large source size.

The measurement of the space-time extent of the particle emitting region has been one of the important goals in high-energy experiments for several decades [3–5]. These measurements are based on the sensitivity of particle-momentum correlations to the space-time separation of the particle emitters due to the effects of quantum statistics (QS) and final-state interaction (FSI). For identical particles, the QS symmetrization (antisymmetrization) is usually the dominant source of the correlation and, due to the interference of the amplitudes corresponding to various permutations of identical particles, this measurement is often called particle interferometry (see Ref. [6] for a review).

Most of the particles produced in relativistic heavy-ion collisions are pions and, as a result, pion interferometry has been a particularly useful tool in correlation studies. High statistics data from colliders like RHIC have also made it possible to study kaon correlations. In this article, we present the first results on two- K_s^0 correlations in central Au+Au collisions at $\sqrt{s_{NN}} = 200$ GeV measured by the STAR (Solenoidal Tracker at RHIC) experiment at RHIC.

It is known that a significant fraction of pions come from resonance decays after freeze-out, thus complicating the pion interferometry measurements. Although the direct pion source may be inherently non-Gaussian, the resonances extend the source size due to their finite lifetime, introduce an additional essentially non-Gaussian distortion in the two-pion correlator and reduce the fitted correlation strength. Due to the limited decay momenta, the decay pions populate mainly the low-momentum region, thus introducing an additional pair momentum dependence in the correlator.

Kaon interferometry, however, suffers less from resonance contributions and could provide a cleaner signal for correlation studies than pions [7,8]. Higher multiparticle correlation effects that might play a role for pions should be of minor importance for kaons because the kaon density is considerably smaller than the pion density at RHIC ($\sqrt{s_{NN}} = 200$ GeV). The pion multiplicity has increased by approximately 70% from the SPS ($\sqrt{s_{NN}} = 17.3$ GeV) to RHIC [9]. The interferometry radii, however, remain almost the same [10,11]. The strangeness distillation mechanism [12] might further increase any time delay QGP signature. This mechanism could lead to strong temporal emission asymmetries between kaons and antikaons [13], thus probing the latent heat of the phase transition.

Particle identification for pions, via their specific ionization (energy loss per unit length or dE/dx), works only up to about 700 MeV/c. Neutral kaons, however, can be identified up to much higher momentum using their decay topology. This allows for the extension of the interferometry systematics to a higher momentum than is presently achievable with pions and thus provide a means to probe the earlier times of the collision. The effect of two-track resolution, which is a limiting factor in charged-particle correlations, is also small. The absence of Coulomb FSI suppression together with small contributions

from resonance decays make neutral kaon correlations a powerful tool to investigate the space-time structure of the particle-emitting source.

The OPAL [14] and ALEPH [15] collaborations have measured correlations of neutral kaons from hadronic decays of Z^0 in e^+e^- collisions at Large Electron Positron Collider (LEP). The WA97 experiment at CERN [16] attempted to measure $K_s^0 K_s^0$ correlations but did not see a significant enhancement of neutral kaon pairs in the region of small-momentum difference due to a lack of sufficient statistics.

II. THE STAR EXPERIMENT

The STAR detector [17] consists of several detector subsystems in a large solenoidal magnet that provides a uniform 0.5-T field. For the data used in this analysis, the main setup consisted of the time projection chamber (TPC) [18] for charged-particle tracking, a scintillator trigger barrel (CTB) surrounding the TPC for measuring charged-particle multiplicity, and two zero-degree calorimeters (ZDC) [19] located upstream and downstream along the axis of the TPC and beams to detect spectator neutrons. With full azimuthal coverage over $|\eta| < 1$ and an almost 100% efficiency for minimum ionizing particles, the CTB provides a good estimate of the number of charged particles produced in the mid-rapidity region. The number of neutrons detected in the ZDC's is identified with the amount of energy deposited in them. The collision centrality is determined by correlating the energy deposition in the ZDC with the number of minimum ionizing particles detected by the CTB.

A. Data selection

For this analysis, events from the ZDC and CTB central trigger (0–10% of the total hadronic cross section) data sets were used with an event vertex within ± 25 cm of the center of the TPC, along the beam axis. Approximately 2.5×10^6 events with about $3K_s^0$ per event on the average were analyzed. Here we discuss K_s^0 -specific issues only, as details of pion interferometry at the STAR experiment have been discussed in Ref. [20]. The K_s^0 has a mean decay length ($c\tau$) of 2.7 cm and decays via the weak interaction into π^+ and π^- with a branching ratio of about 68%. The mass and kinematic properties of the K_s^0 are determined from the decay vertex geometry and daughter-particle kinematics [21]. Neutral kaon candidates are formed out of a pair of positive and negative tracks whose trajectories point to a common secondary decay vertex that is well separated from the primary event vertex. All neutral kaon candidates, with invariant masses from 0.48 to 0.51 GeV/ c^2 , transverse momentum from 0.5 to 3.5 GeV/ c , and rapidity between -1.5 and 1.5 have been considered. The daughter-particle tracks are required to have a minimum of 15 TPC hits and a distance of closest approach to the primary vertex greater than 1.3 cm.

B. The correlation function

Experimentally, the two-particle correlation function is defined as

$$C_2(Q) = \frac{A(Q)}{B(Q)}, \quad (1)$$

where $A(Q)$ represents the distribution of the invariant relative momentum $Q = \sqrt{-q^\mu q_\mu}$, $q^\mu = p_1^\mu - p_2^\mu$, for a pair of particles from the same event. The possibility of a single neutral kaon being correlated with itself, i.e., correlation between a real K_s^0 and a fake K_s^0 reconstructed from a pair that shares a daughter of the real K_s^0 , was eliminated by requiring that kaons in a pair have unique daughters. We have also explored effects from splitting of daughter tracks by looking at the angular correlation between the normal vectors to the decay planes of the K_s^0 in a given pair. No enhancement at very small angles was observed indicating no significant problem from track splitting. $B(Q)$ is the reference distribution constructed by mixing particles from different events with similar Z -vertex positions (relative z position within 5 cm). The individual K_s^0 for a given mixed pair are required to pass the same single particle cuts applied to those that go into the real pairs. The mixed pairs are also required to satisfy the same pairwise cuts applied to the real pairs from one event. The efficiency and acceptance effects cancel out in the ratio $A(Q)/B(Q)$.

C. Data analysis

Figure 1 shows the invariant mass distribution of the neutral kaons based on the set of cuts described above. The background is characterized by a polynomial fit to the distribution outside the mass peak. The observed mass $495.6 \pm 6.8 \text{ MeV}/c^2$ is consistent with the accepted value [22]. The signal and background for the mass range from 0.48 to 0.51 GeV/c^2 considered in this analysis are shown by the shaded regions.

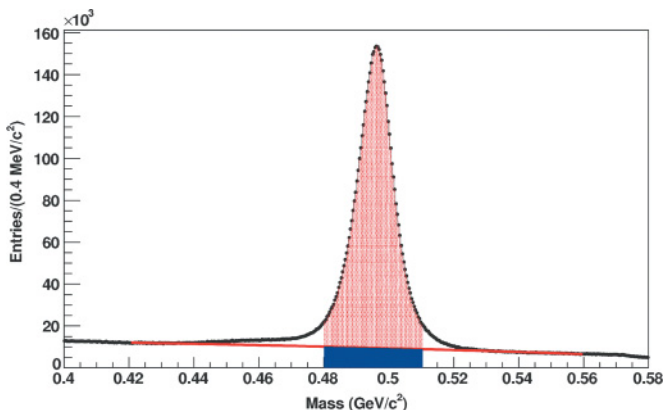


FIG. 1. (Color online) The K_s^0 invariant mass distribution from central Au+Au collisions at $\sqrt{s_{NN}} = 200 \text{ GeV}$. The range in transverse momentum is from 0.5 to 3.5 GeV/c and rapidity is between -1.5 and 1.5 . Kaon candidates falling in the mass range from 0.48 to 0.51 GeV/c^2 , indicated by the shaded region, were selected for this correlation study. The corresponding mass is $495.6 \pm 6.8 \text{ MeV}/c^2$.

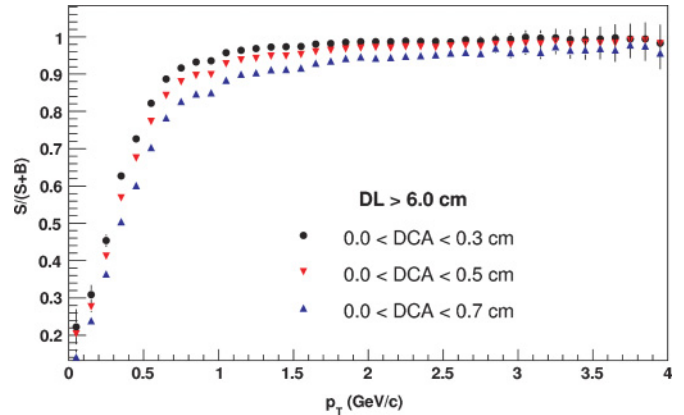


FIG. 2. (Color online) The K_s^0 signal to (signal+background) ratio as a function of the transverse momentum p_T . The data points correspond to a decay length (DL) greater than 6 cm. The kaons selected fall in the mass range from 0.48 to 0.51 GeV/c^2 , which is also the mass range for the correlation analysis. The errors are only statistical.

After tuning several kinematical and detector related cuts to remove most of the background, some residual background still remains. This calls for a knowledge of the signal-to-background ratio within the selected invariant mass range to make corrections to the measured correlation function. For neutral kaons, the decay length (DL) and distance of closest approach (DCA) to the interaction vertex were two of the parameters for which it was difficult to determine where to apply the cuts. Various DCA and DL cut combinations were investigated by varying the DCA from 0.3 to 0.8 cm in steps of 0.1 cm and the DL from 2.0 to 6.0 cm in steps of 1.0 cm. Figure 2 displays an example of the signal-to-background ratio as a function of p_T for $DL > 6 \text{ cm}$ and various DCA values. The single-particle purity gets worse as the DCA gets larger for the given DL cut. If one instead looks at a fixed DCA and varies the DL cut instead, the purity gets better with increasing decay length.

The effect of momentum resolution on the correlation functions has also been investigated using simulated tracks from K_s^0 decays with known momenta, \vec{p}_{in} , embedded into real events. The embedded tracks were simulated taking into account the response of the TPC and scattering effects. The reconstructed momenta of the embedded tracks, \vec{p}_{rec} , are then compared with \vec{p}_{in} . The distributions of $|\vec{p}_{rec} - \vec{p}_{in}|/|\vec{p}_{in}|$ with respect to \vec{p}_{in} are then fit to Gaussians to obtain the RMS widths. These are used to characterize the momentum resolution of the detector. The resolution in p lies between 1 and 2% for the p_T range used in this analysis.

The top panel in Figure 3 shows the K_T distribution for $Q < 0.2 \text{ GeV}/c$ where $K_T = (|\vec{p}_{1T} + \vec{p}_{2T}|)/2$. The corresponding number of pairs for the distribution with low pair purity is approximately 1.92×10^4 and that for the one with the high pair purity is about 5.5×10^3 . The distribution in the bottom panel corresponds to pairs with $Q < 0.1 \text{ GeV}/c$, with 2.7×10^3 pairs for the low pair purity distribution and 7.8×10^2 for the high pair purity distribution. It is clear that the shape of the K_T distribution changes with the pair purity and, as a result, so

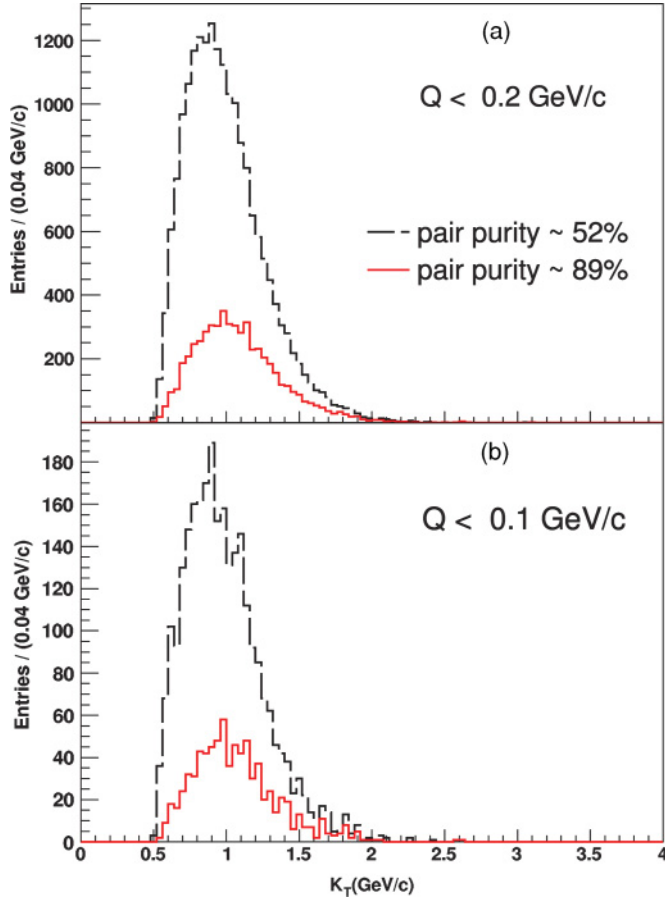


FIG. 3. (Color online) The K_T distribution of the K_s^0 pairs. The range in transverse momentum of the single particles is from 0.5 to 3.5 GeV/c. The distribution in (a) corresponds to $Q < 0.2$ GeV/c and that in (b) is for $Q < 0.1$ GeV/c, i.e., (b) is a subset of (a). The two histograms in each panel are for low (dashed) and high (full) pair purity.

does $\langle K_T \rangle$, the mean of the distribution. The mean K_T varies almost linearly with pair purity. For the lowest pair purity value of $\approx 52\%$, $\langle K_T \rangle \approx 0.805$ GeV/c. At the highest pair purity value of $\approx 89\%$, $\langle K_T \rangle \approx 1.07$ GeV/c. The dependence of $\langle K_T \rangle$ on the pair purity together with the fact that the radii may vary with K_T implies that varying the pair purity may change the measured radii. In this analysis, the correlation function is integrated over all K_T because the statistics are not sufficient to make a K_T -dependent study.

Corrections to the raw correlation functions were applied according to the expression

$$C_{\text{corrected}}(Q) = \frac{C_{\text{measured}}(Q) - 1}{\text{PairPurity}(Q)} + 1, \quad (2)$$

where the pair purity was calculated as the product of the signal(S) to signal plus background ($S + B$) ratios of the two K_s^0 of the pair (i,j)

$$\text{PairPurity}(Q) = \frac{S}{S+B}(p_{ii}) \times \frac{S}{S+B}(p_{jj}) \quad (3)$$

The pair purity, $\text{PairPurity}(Q)$, has been found to be independent of Q over the range of invariant four-momentum

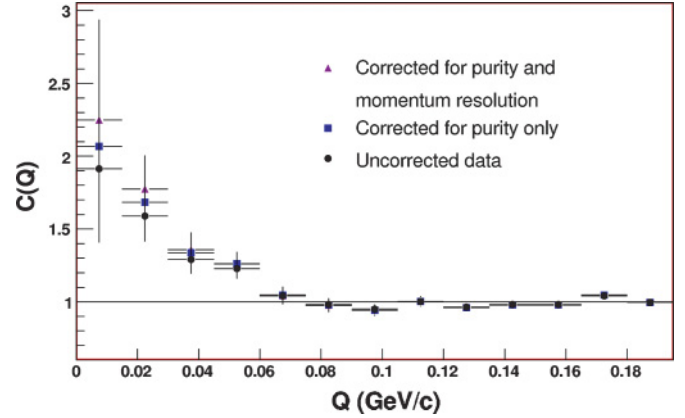


FIG. 4. (Color online) The $K_s^0 K_s^0$ correlation function from central Au+Au collisions at $\sqrt{s_{NN}} = 200$ GeV. The solid circles are for uncorrected data. The squares correspond to the case where the data have been corrected for pair purity. The triangles represent the data after correcting for pair purity and momentum resolution. The errors are statistical only.

difference considered. As a result, an average value over Q of the pair purity has been used to correct the correlation function for each set of cuts considered.

Figure 4 shows the experimental $K_s^0 K_s^0$ correlation function before and after corrections for purity and momentum resolution are applied. We have verified that the correlation function due to pairs coming outside the K_s^0 mass window is flat. It can be seen that the effect of momentum resolution is comparable to that of purity correction. The one-dimensional correlation function is usually fitted to a Gaussian

$$C(Q) = N \cdot (1 + \lambda \cdot e^{-R^2 Q^2}) \quad (4)$$

where N and R are, respectively, the normalization and size parameter, the latter characterizing the width of the Gaussian distribution of the vector \vec{r}^* of the relative distance between particle emission points in the pair center-of-mass (c.m.) system:

$$\frac{d^3 N}{d^3 \vec{r}^*} \propto e^{-\vec{r}^{*2}/(4R^2)}. \quad (5)$$

The parameter λ measures the correlation strength. In the absence of FSI, λ equals unity for a fully chaotic Gaussian source, up to a suppression due to the kaon impurity and finite momentum resolution. Theoretically, it can be less than unity due to partial coherence of the kaon field, resonance decays and the non-Gaussian form of the correlation function. Also neglecting FSI can affect (suppress or enhance) the value of this parameter.

III. FINAL-STATE INTERACTION IN THE NEUTRAL KAON SYSTEM

The production of the neutral kaon system, K^0 and \bar{K}^0 , is attributed to the strong interaction that conserves the strangeness quantum number. An interesting property of neutral kaons is that the K^0 can change into a \bar{K}^0 through a second-order weak interaction. However, the particles that

we normally observe through weak decay channels in the laboratory are not K^0 and \bar{K}^0 [23]. Neglecting the effects of CP violation, the observed weak interaction eigenstates are given by

$$\begin{aligned} |K_s^0\rangle &= \frac{1}{\sqrt{2}}(|K^0\rangle + |\bar{K}^0\rangle), \\ |K_l^0\rangle &= \frac{1}{\sqrt{2}}(|K^0\rangle - |\bar{K}^0\rangle), \end{aligned} \quad (6)$$

where $|K_s^0\rangle$ and $|K_l^0\rangle$ are the state vectors of the short- and long-lived neutral kaons, to which experiments have access via measurements of their decay products, which are mainly pions. The state vector of the $K_s^0 K_s^0$ system is then given by the expression

$$\begin{aligned} |K_s^0 K_s^0\rangle &= \frac{1}{2}(|K^0 K^0\rangle + |K^0 \bar{K}^0\rangle \\ &\quad + |\bar{K}^0 K^0\rangle + |\bar{K}^0 \bar{K}^0\rangle). \end{aligned} \quad (7)$$

Now, if a $K_s^0 K_s^0$ pair comes from $K^0 K^0 (\bar{K}^0 \bar{K}^0)$, it is subject to Bose-Einstein (BE) enhancement as it originates from an identical boson pair. However, the K^0 and \bar{K}^0 are two different particles and one may not expect correlations if one K_s^0 comes from K^0 and the other one from \bar{K}^0 . Nevertheless, it can be shown [24] (see also Refs. [25–27]) that only the symmetric part of the $K^0 \bar{K}^0$ amplitude contributes to the $K_s^0 K_s^0$ system and thus also leads to a Bose-Einstein enhancement at small relative momentum (on the contrary, only the anti-symmetric part of the $K^0 \bar{K}^0$ amplitude contributes to the $K_s^0 K_l^0$ system and leads to the ‘‘Fermi-Dirac like’’ suppression). The $K_s^0 K_s^0$ correlation thus includes a unique interference term that may provide additional space-time information. Here only the $K_s^0 K_s^0$ correlation is considered because most of the K_l^0 decay outside the STAR TPC and are not accessible.

The strong FSI has an important effect on neutral kaon correlations due to the near threshold resonances, $f_0(980)$ and $a_0(980)$ [28]. These resonances contribute to the $K^0 \bar{K}^0$ channel and lead to the s -wave scattering length dominated by the imaginary part of ~ 1 fm. Based on the predictions of chiral perturbation theory for pions [29] the nonresonant s -wave scattering lengths are expected to be ~ 0.1 fm for both $\bar{K}^0 \bar{K}^0$ and $K^0 K^0$ channels and can be neglected to a first approximation.

To calculate the $K_s^0 K_s^0$ correlation function, we assume K^0 's and \bar{K}^0 's emitted by independent single-kaon sources so that the fraction of $K_s^0 K_s^0$ pairs originating from $K^0 \bar{K}^0$ system is $\alpha = (1 - \epsilon^2)/2$, where ϵ is the $K^0 - \bar{K}^0$ abundance asymmetry. We have put $\alpha = 1/2$ based on the negligible $K^+ - K^-$ abundance asymmetry of 0.018 ± 0.106 as measured under the same conditions by the STAR experiment [30]. The correlation function is calculated as a mixture of the average squares of the properly symmetrized $K^0 K^0$, $\bar{K}^0 \bar{K}^0$ and nonsymmetrized $K^0 \bar{K}^0$ wave functions, weighted by the respective $K_s^0 K_s^0$ fractions. To average over the relative distance vector \vec{r}^* , we use the Lednický and Lyuboshitz analytical model [28], assuming \vec{r}^* is distributed according to Eq. (5) with a Gaussian radius R . The model assumes that the nonsymmetrized wave functions $\Psi_{-\vec{k}^*}(\vec{r}^*)$ describing the elastic transitions can be written as a superposition of the plane and spherical waves,

the latter being dominated by the s -wave,

$$\Psi_{-\vec{k}^*}(\vec{r}^*) = e^{-i\vec{k}^* \cdot \vec{r}^*} + f(k^*) \frac{e^{ik^* r^*}}{r^*}, \quad (8)$$

where $\vec{k}^* \equiv \vec{Q}/2$ is the three-momentum of one of the kaons in the pair rest frame and $f(k^*)$ is the s -wave scattering amplitude for a given system. Neglecting the scattered waves for the $K^0 K^0$ and $\bar{K}^0 \bar{K}^0$ systems [the corresponding $f(k^*) = 0$] one obtains the following expression for the $K_s^0 K_s^0$ correlation function [28]:

$$\begin{aligned} C(Q) &= 1 + e^{-Q^2 R^2} + \alpha \left[\left| \frac{f(k^*)}{R} \right|^2 \right. \\ &\quad \left. + \frac{4\Re f(k^*)}{\sqrt{\pi} R} F_1(QR) - \frac{2\Im f(k^*)}{R} F_2(QR) \right], \end{aligned} \quad (9)$$

where $F_1(z) = \int_0^z dx e^{x^2 - z^2}/z$ and $F_2(z) = (1 - e^{-z^2})/z$. The s -wave $K^0 \bar{K}^0$ scattering amplitude $f(k^*)$ is dominated by the near threshold s -wave isoscalar and isovector resonances $f_0(980)$ and $a_0(980)$, characterized by their masses m_r and respective couplings γ_r and γ'_r to the $K \bar{K}$, $\pi\pi$ and $K \bar{K}$, $\pi\eta$ channels. Associating the amplitudes f_I at isospin $I = 0$ and $I = 1$ with the resonances $r = f_0$ and a_0 respectively, one can write [28,31]

$$f(k^*) = [f_0(k^*) + f_1(k^*)]/2, \quad (10)$$

$$f_I(k^*) = \gamma_r / [m_r^2 - s - i\gamma_r k^* - i\gamma'_r k'_r]. \quad (11)$$

Here $s = 4(m_K^2 + k^{*2})$ and k'_r denotes the momentum in the second ($\pi\pi$ or $\pi\eta$) channel with the corresponding partial width $\Gamma'_r = \gamma'_r k'_r / m_r$.

There is a great deal of uncertainty in the properties of these resonances due to insufficiently accurate experimental data and the different approaches used in their analysis. Fortunately, the dominant imaginary part of the scattering amplitude is basically determined by the ratios of the $f_0 K \bar{K}$ to $f_0 \pi\pi$ and $a_0 K \bar{K}$ to $a_0 \pi\eta$ couplings whose variation is rather small [32]. In this article we use the resonance masses and couplings from (a) Martin *et al.* [31], (b) Antonelli [33], (c) Achasov *et al.* [34], (d) Achasov *et al.* [34] (see Table I) to demonstrate the impact of their characteristic uncertainties on the calculated correlation function.

We have taken into account the normalization and correlation strength parameters N and λ by the substitution $C(Q) \rightarrow N \cdot [\lambda \cdot C(Q) + (1 - \lambda)]$. Following Ref. [35], we have also included a small contribution of the inelastic transition between the coupled-channels $K^+ K^- (\equiv 2)$ and $K^0 \bar{K}^0 (\equiv 1)$ (see Appendix for more details). In addition to a direct contribution of the average square of the corresponding wave function $\Psi_{-\vec{k}^*}^{21}(\vec{r}^*)$ given in Eq. (12), this transition also leads to a modification of the amplitude $f(k^*)$ in the wave function of the elastic transition in Eq. (8). Instead of Eq. (10), this amplitude is now represented by the element f_c^{11} of a 2×2 matrix \hat{f}_c defined in Eq. (13). We have further considered the correction $\Delta C_{K\bar{K}}$ in Eq. (16) due to the deviation of the spherical waves from the true scattered waves in the inner region of the short-range potential, which is of comparable size to the effect of the second channel.

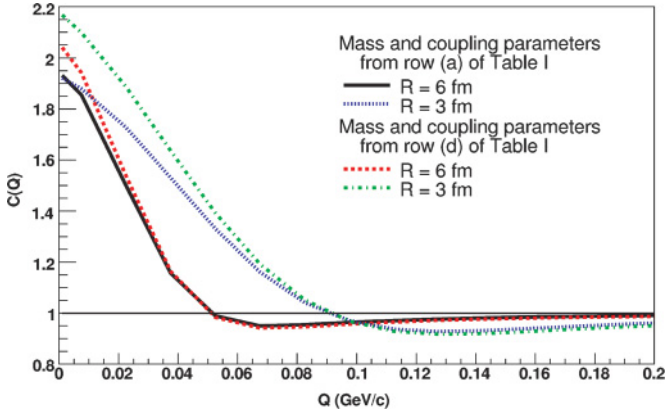


FIG. 5. (Color online) Theoretical correlation functions for input Gaussian sources of $R = 6$ fm and $R = 3$ fm with $\lambda = 1$, $N = 1$. The resonance masses and coupling constants are from Table I.

Figure 5 shows the theoretical correlation functions for two sets of resonance parameters from Table I with $R = 6$ and $R = 3$ fm as input radii with the normalization factor N and λ both set to unity.

The results indicate that the effect of the strong FSI in the $K^0\bar{K}^0$ system is to give rise to a repulsive-like component causing the correlation function to go below unity.

IV. EXPERIMENTAL RESULTS

The experimental correlation functions are fit using the Lednický and Lyuboshitz [28] model to take into account the effect of the strong FSI. The free parameters are the radius R characterizing the separation \vec{r}^* of the particle emission points in the pair rest frame, the normalization N , and λ . This fitting was done assuming the Gaussian \vec{r}^* -distribution of Eq. (5).

The fit results are summarized in Table II for various sets of resonance parameters. The normalization $N = 1.03$ in all cases. The difference between the single-channel and coupled-channel fits is very small, but it is the coupled channel fit results which are more accurate. Figure 6 shows an example of the model fits to the experimental correlation function. The average confidence level for the FSI fits is 70.5% and the Gaussian fit has a confidence level of 38%. One can see that a simple Gaussian fit cannot account for the $C(Q) < 1$ part of the data that are fit better if the strong FSI is included. Figures 7 and 8 show the dependence of the extracted R_{inv} and λ parameters as a function of the PairPurity before, (a), and after, (b), correcting for this impurity. The data points are not

TABLE I. The f_0 and a_0 masses and coupling parameters, all in GeV, from (a) Martin *et al.* [31], (b) Antonelli *et al.* [33], (c) Achasov *et al.* [34] and (d) Achasov *et al.* [34].

Reference	m_{f_0}	$\gamma_{f_0 K \bar{K}}$	$\gamma_{f_0 \pi \pi}$	m_{a_0}	$\gamma_{a_0 K \bar{K}}$	$\gamma_{a_0 \pi \eta}$
a	0.978	0.792	0.199	0.974	0.333	0.222
b	0.973	2.763	0.5283	0.985	0.4038	0.3711
c	0.996	1.305	0.2684	0.992	0.5555	0.4401
d	0.996	1.305	0.2684	1.003	0.8365	0.4580

TABLE II. The values of the radius R in fm and the suppression parameter λ obtained by fitting the $K_s^0 K_s^0$ experimental correlation function with the model [28] that takes into account the FSI effect in the resonance ($f_0 + a_0$) approximation. The normalization $N = 1.03$ in all cases. The values correspond to the third set of points from the right in Figure 7, so chosen as to strike a balance between statistics and purity. The results in the first and the second column respectively correspond to the single- and two-channel fits. The errors are, from left to right, statistical and systematic errors introduced by the uncertainty on the purity correction. The systematic errors from the model fits are very small in comparison and are not shown.

R_{inv} (fm)	One-ch. fit	Two-ch. fit
a	$3.90 \pm 0.45 \pm 0.37$	$4.07 \pm 0.46 \pm 0.31$
b	$3.89 \pm 0.44 \pm 0.35$	$4.09 \pm 0.46 \pm 0.31$
c	$3.96 \pm 0.45 \pm 0.34$	$4.14 \pm 0.47 \pm 0.31$
d	$3.91 \pm 0.44 \pm 0.34$	$4.07 \pm 0.45 \pm 0.29$
λ	One-ch. fit	Two-ch. fit
a	$0.89 \pm 0.21 \pm 0.10$	$0.98 \pm 0.24 \pm 0.14$
b	$0.83 \pm 0.20 \pm 0.10$	$0.93 \pm 0.23 \pm 0.13$
c	$0.81 \pm 0.20 \pm 0.09$	$0.90 \pm 0.23 \pm 0.12$
d	$0.78 \pm 0.19 \pm 0.09$	$0.86 \pm 0.22 \pm 0.12$

independent of each other as low-purity data may contain some or all of the high-purity data. The fit results are not sensitive to the resonance parameters used. Hence, the systematic errors are driven by the data and not theory. Figure 7 shows only a slight dependence of the radius parameter on the pair purity. However, λ in Figure 8(a) has a strong dependence on pair purity. Even though the purity correction seems to improve the results, there is still a slight dependence remaining as shown in Figure 8(b). The value of λ for the data with the highest purity, and therefore the cleanest signal, is consistent with unity. This is expected for a chaotic system with little contributions from decaying resonances. Plotting the radius as a function of the mean K_T , as shown in Figure 9, shows a slight dependence of R with increasing K_T . However, this

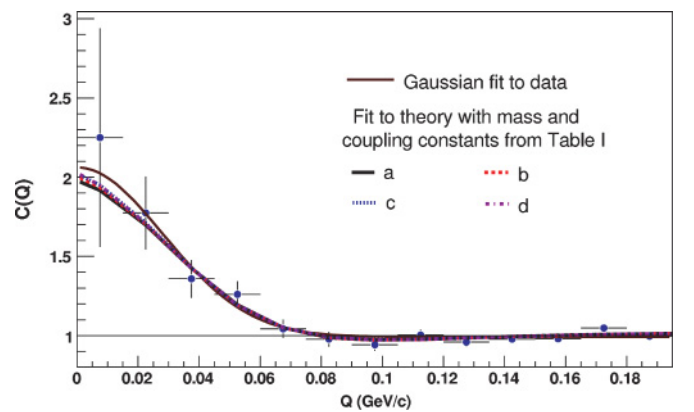


FIG. 6. (Color online) Fits to the $K_s^0 K_s^0$ experimental correlation function, including the strong interaction with resonance masses and coupling constants from Table I. The confidence levels for the FSI fits are (a) 71%, (b) 70%, (c) 70%, and (d) 71%. A simple Gaussian fit, with a confidence level of 38%, is also shown for comparison. The errors are only statistical.

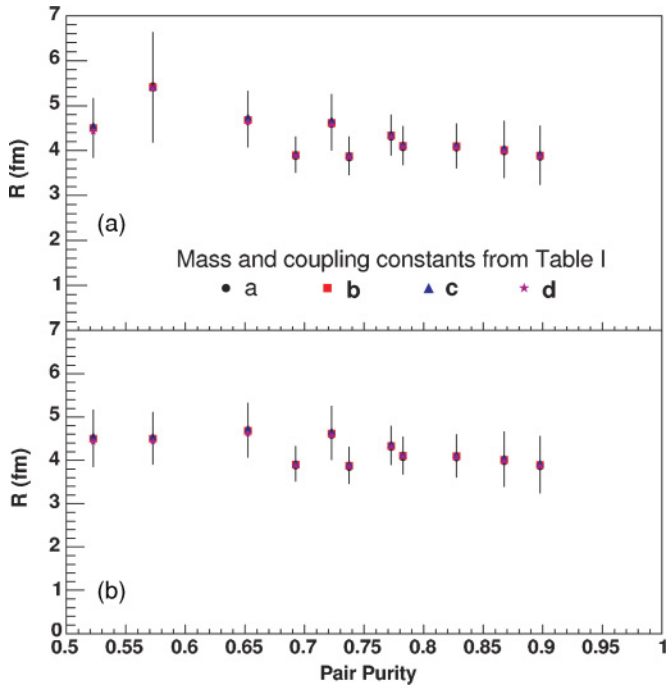


FIG. 7. (Color online) The extracted R as a function of the pair purity (a) before correction for purity and (b) after correction for purity. The errors are only statistical.

could be a remaining artifact of the mean K_T dependence on pair purity, as mentioned earlier and shown in Figure 3. One has to look at several K_T bins for a specified pair purity to study a K_T dependence of the radius coming from

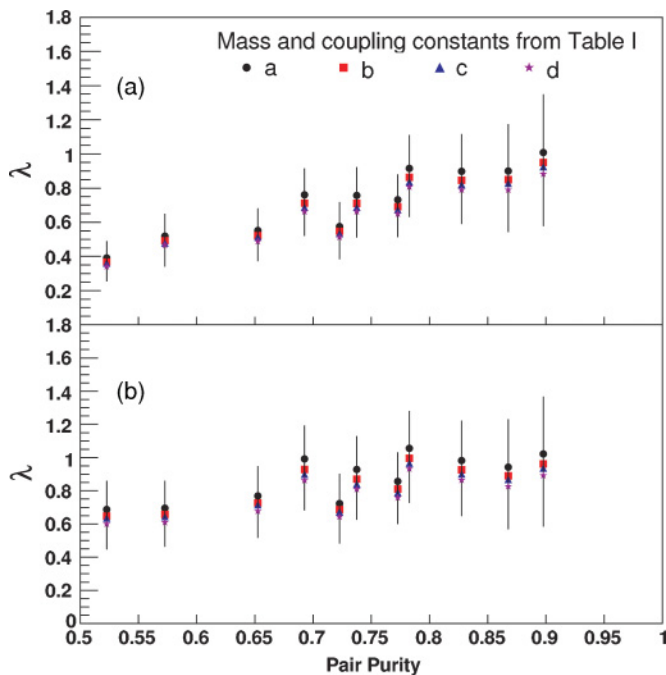


FIG. 8. (Color online) The extracted λ as a function of the pair purity (a) before correction for purity and (b) after correction for purity. The errors are only statistical.

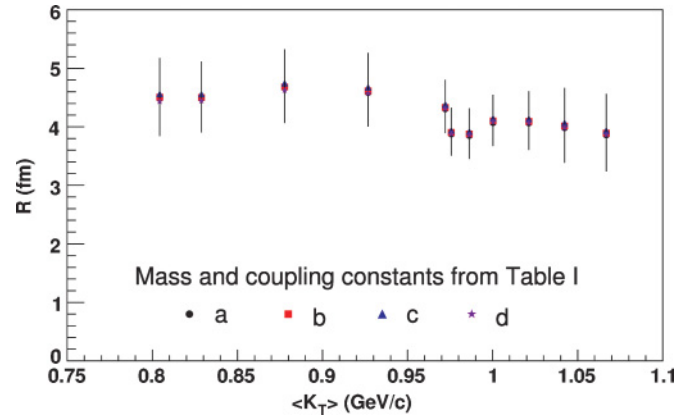


FIG. 9. (Color online) The extracted R as a function of the mean K_T of the pairs that go into the correlation function. The errors are only statistical.

real physics effects. This was not possible in this analysis due to the limited statistics. To strike a balance between statistics and purity, we averaged over the data from the coupled-channel analysis corresponding the third set of points from the right in Figure 7(b), with a pair purity of $\approx 82\%$, to obtain the values $R = 4.09 \pm 0.46(\text{stat}) \pm 0.31(\text{sys})$ fm and $\lambda = 0.92 \pm 0.23(\text{stat}) \pm 0.13(\text{sys})$ at the mean transverse mass $\langle m_T \rangle = 1.07$ GeV.

Figure 10 shows the m_T dependence of R extracted from $\pi\pi$ [20], $K_s^0 K_s^0$, and proton- Λ correlations [36]. Considering the large mean transverse momentum of the pair, the value of R for K_s^0 before taking into account the FSI in the $K^0 \bar{K}^0$ system is larger than expected from the systematics followed by the rest of the data. However, after taking into account the FSI effect the neutral kaons also seem to follow the m_T scaling that hydrodynamics predicts [37].

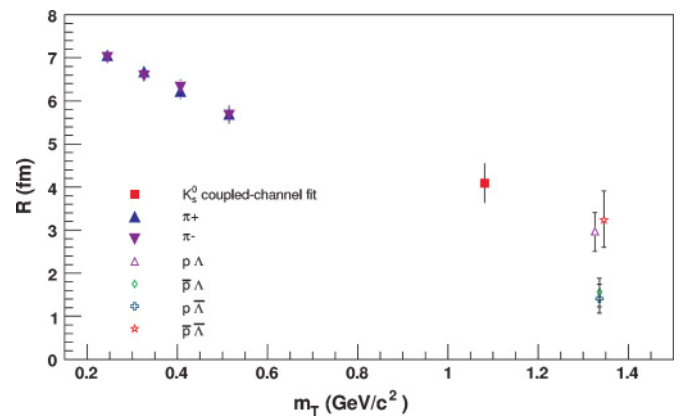


FIG. 10. (Color online) R as a function of m_T in central Au+Au collisions at $\sqrt{s_{NN}} = 200$ GeV. Statistical and systematic errors are shown. The FSI uncertainty measured by the spread of the fit results in rows (a)–(d) of Table II is substantially smaller than the statistical error.

V. CONCLUSIONS

We have presented the first measurement of neutral kaon correlations in heavy-ion collisions at RHIC at $\sqrt{s_{NN}} = 200$ GeV. One has to consider the effects of FSI to obtain reasonable agreement between theory and data. The variations of the resonance parameters result in very small differences, which are well within our systematic errors. The effect of the pair purity on the correlation function has been studied extensively and is well understood. A Gaussian fit to the correlation function does not account very well for the $C(Q) < 1$ part of the data and gives a radius which is larger compared to the model fit results.

The measured correlation radius is intermediate between those obtained from two-pion and proton-lambda correlations in these collisions with the same conditions except for a different transverse mass, m_T . The radii seem to follow a universal m_T dependence in agreement with a universal collective flow predicted by hydrodynamics. The value of the parameter λ , based on the high-purity data, is consistent with unity and thus points to a chaotic kaon source. This is in correspondence with an indication of a dominantly chaotic pion source obtained from STAR measurement of three pion correlations [38].

Our results represent an important first step toward a multidimensional analysis of neutral kaon correlations using the high statistics data from RHIC. In the future this analysis will allow the extraction of information about the freeze-out geometry, collective flow velocity, the evolution time, and duration of particle emission. The latter is especially interesting in the context of an increased emission duration expected if there is a first-order phase transition from a quark gluon plasma to a hadronic system. Recent pion interferometry measurements at RHIC, however, point to a smaller evolution time and emission duration than expected from the usual hydrodynamic and transport models. This result may indicate an explosive character of the collision and is often considered the interferometry puzzle. The fact that the Coulomb interaction is absent in the dominant elastic transition and that the FSI effect can be handled with sufficient accuracy makes neutral kaon interferometry a powerful tool that allows for an important cross-check of charged pion correlation measurements. Pion measurements are much more strongly affected by contributions from resonance decays and final-state interactions.

ACKNOWLEDGMENTS

We thank the RHIC Operations Group and RCF at BNL, and the NERSC Center at LBNL for their support. This work was supported in part by the Offices of NP and HEP within the U.S. DOE Office of Science; the U.S. NSF; the BMBF of Germany; CNRS/IN2P3, RA, RPL, and EMN of France; EPSRC of the United Kingdom; FAPESP of Brazil; the Russian Ministry of Science and Technology; the Ministry of Education and the NNSFC of China; IRP and GA of the Czech Republic, FOM of the Netherlands, DAE, DST, and CSIR of the Government of India; Swiss NSF; the Polish State

Committee for Scientific Research; SRDA of Slovakia, and the Korea Science & Engineering Foundation.

APPENDIX

The interaction of final-state particles can proceed not only through the elastic transition $ab \rightarrow ab$ but also through inelastic reactions of the type $cd \rightarrow ab$, where c and d are also final-state particles of the production process. The FSI effect on particle correlations is known to be significant only for particles with a slow relative motion. Such particles continue to interact with each other after leaving the domain of particle production and their slow relative motion guarantees the possibility of the separation (factorization) of the amplitude of a slow FSI from the amplitude of a fast production process. For the relative motion of the particles involved in the FSI to be slow, the sums of the particle masses in the entrance and exit channels should be close to each other [35]. Thus, in our case, one should account for the effect of inelastic transition $K^+K^- \rightarrow K^0\bar{K}^0$ in addition to the elastic transition $K^0\bar{K}^0 \rightarrow K^0\bar{K}^0$. Instead of a single-channel Schrödinger equation one should thus solve a two-channel one. In solving the standard scattering problem, one should take into account that the FSI problem corresponds to the inverse direction of time. As a result, one has to make the substitution $\vec{k}^* \rightarrow -\vec{k}^*$ and consider $K^0\bar{K}^0 (\equiv 1)$ as the entrance channel and $K^+K^- (\equiv 2)$ as the exit channel. Because the particles in both channels are members of the same isospin multiplets, one can assume that they are produced with about the same probability. Therefore the correlation function will be simply a sum of the average squares of the wave functions $\Psi_{-\vec{k}^*}^{11}(\vec{r}^*)$ and $\Psi_{-\vec{k}^*}^{21}(\vec{r}^*)$ describing the elastic and inelastic transitions, respectively.

Assuming the s -wave dominance and r^* outside the range of the strong interaction potential, one has [35]

$$\Psi_{-\vec{k}^*}^{21}(\vec{r}^*) = f_c^{21}(k^*) \sqrt{\frac{\mu_2}{\mu_1}} \frac{\tilde{G}(\rho_2, \eta_2)}{r^*}, \quad (12)$$

where $\mu_1 = m_{K^0}/2$ and $\mu_2 = m_{K^+}/2$ are the respective reduced masses in the two channels. $\rho_2 = k_2^* r^*$, $\eta_2 = (k_2^* a_2)^{-1}$ and $k_2^* = [2\mu_2(k^{*2}/(2\mu_1) + 2m_{K^0} - 2m_{K^+})]^{1/2}$ is the K^+ momentum in the two-kaon rest frame. $a_2 = -(\mu_2 e^2)^{-1} = -109.6$ fm is the (negative) K^+K^- Bohr radius, $f_c^{21}(k^*)$ is the s -wave transition amplitude renormalized by Coulomb interaction in the K^+K^- channel, $\tilde{G}(\rho, \eta) = \sqrt{A_c(\eta)} [G_0(\rho, \eta) + iF_0(\rho, \eta)]$ is the combination of the singular and regular s -wave Coulomb functions G_0 and F_0 . Finally $A_c(\eta) = 2\pi\eta/[\exp(2\pi\eta) - 1]$ is the Coulomb penetration (Gamow) factor.

The wave function of the elastic transition $1 \rightarrow 1$ is still given by Eq. (8) in which $k^* \equiv k_1^*$ and the amplitude $f = f_c^{11}$ is now the element of a 2×2 matrix

$$\hat{f}_c = (\hat{K}^{-1} - i\hat{k}_c)^{-1}. \quad (13)$$

Here \hat{K} is a symmetric matrix and \hat{k}_c is a diagonal matrix in the channel representation: $k_c^{11} = k^*$, $k_c^{22} = A_c(\eta_2)k_2^* - 2ih(\eta_2)/a_2$, where the function $h(\eta)$ is expressed through the digamma function $\psi(z) = \Gamma'(z)/\Gamma(z)$ as $h(\eta) = [\psi(i\eta) - \psi(-i\eta) - \ln \eta^2]/2$. Assuming that the isospin violation arises

solely from the mass difference and Coulomb effects on the element k_c^{22} , making it different from the momentum k^* in the neutral kaon channel, one can express the \hat{K}^{-1} matrix, in the channel representation through the inverse diagonal elements K_I^{-1} of the \hat{K} matrix in the representation of total isospin I (the products of the corresponding Clebsch-Gordan coefficients being 1/2 or $-1/2$):

$$\begin{aligned} (\hat{K}^{-1})^{11} &= (\hat{K}^{-1})^{22} = \frac{1}{2}[K_0^{-1} + K_1^{-1}], \\ (\hat{K}^{-1})^{21} &= (\hat{K}^{-1})^{12} = \frac{1}{2}[K_0^{-1} - K_1^{-1}]. \end{aligned} \quad (14)$$

The latter are assumed to be dominated by the resonances $r = f_0(980)$ and $a_0(980)$ for $I = 0$ and 1, respectively, so:

$$K_I^{-1} = (m_r^2 - s - ik_r' \gamma_r') / \gamma_r. \quad (15)$$

One should also take into account the correction $\Delta C_{K\bar{K}}$ due to the deviation of the spherical waves from the true scattered waves in the inner region of the short-range potential, which is of comparable size to the effect of the second channel. This correction is also given in Ref. [35] and is

represented in a compact form in Eq. (125) of Ref. [39]. In our case,

$$\begin{aligned} \Delta C_{K\bar{K}} &= -\frac{1}{4\sqrt{\pi}R^3} [|f_c^{11}|^2 d_0^{11} + |f_c^{11}|^2 d_0^{11} \\ &\quad + 2\Re(f_c^{11} f_c^{21*}) d_0^{21}], \end{aligned} \quad (16)$$

where $d_0^{ij} = 2\Re d(\hat{K}^{-1})^{ij} / dk^{*2}$; at $k^* = 0$, \hat{d}_0 coincides with the real part of the matrix of effective radii.

One may see from Eqs. (9) and (12) that the usual resonance Breit-Wigner behavior settles only at small r^* when squares of the spherical waves $|f_c^{ij}/r^*|^2$ dominate. At sufficiently large k^* , one can neglect the Coulomb effects and put $f_c^{11} \doteq (f_0 + f_1)/2$, $f_c^{21} \doteq (f_0 - f_1)/2$, so that $|f_c^{11}|^2 + |f_c^{21}|^2 \doteq |f_0|^2 + |f_1|^2$. The sum of the square terms then reduces to the incoherent Breit-Wigner contributions of f_0 and a_0 resonances. There can also be additional (not related to FSI) resonance contribution of the usual Briet-Wigner form due to direct $f_0(980)$ and $a_0(980)$ production. This contribution is assumed to be negligible as compared to the FSI effect.

-
- [1] F. Karsch, Z. Phys. C **38**, 147 (1988); Lect. Notes Phys. **583**, 209 (2002).
- [2] S. Pratt, T. Csorgo, and J. Zimanyi, Phys. Rev. C **42**, 2646 (1990).
- [3] M. I. Podgoretsky, Sov. J. Part. Nucl. **20**, 266 (1989).
- [4] U. A. Wiedemann and U. Heinz, Phys. Rep. **319**, 145 (1999).
- [5] R. Lednicky, Phys. At. Nucl. **67**, 72 (2004).
- [6] M. A. Lisa, S. Pratt, R. Soltz, and U. Wiedemann, Annu. Rev. Nucl. Part. Sci. **55**, 357 (2005).
- [7] M. Gyulassy and S. S. Padula, Phys. Rev. C **41**, R21 (1990); Phys. Lett. **B217**, 181 (1989).
- [8] J. P. Sullivan, M. Berenguer, B. V. Jacak, S. Pratt, M. Sarabura, J. Simon-Gillo, H. Sorge and H. van Hecke, Phys. Rev. Lett. **70**, 3000 (1993).
- [9] B. B. Back *et al.* (PHOBOS Collaboration), Phys. Rev. Lett. **85**, 3100 (2000); **88**, 022302 (2002).
- [10] C. Adler *et al.* (STAR Collaboration), Phys. Rev. Lett. **87**, 082301 (2001).
- [11] S. C. Johnson *et al.* (PHENIX Collaboration), Nucl. Phys. **A698**, 603 (2002); W. A. Zajc *et al.*, *ibid.* **A698**, 39 (2002).
- [12] C. Greiner, P. Koch, and H. Stocker, Phys. Rev. Lett. **58**, 1825 (1987); C. Spieles, L. Gerland, H. Stocker, C. Grenier, C. Kuhn, and J. P. Coffin, *ibid.* **76**, 1776 (1996).
- [13] S. Soff *et al.*, J. Phys. G **23**, 2095 (1997); D. Ardouin *et al.*, Phys. Lett. **B446**, 191 (1999).
- [14] G. Abbiendi *et al.* (OPAL Collaboration), Eur. J. Phys. C **21**, 23 (2001).
- [15] D. Buskulic *et al.* (ALEPH Collaboration), Z. Phys. C **64**, 361 (1994).
- [16] F. Antinori *et al.* (WA97 Collaboration), Nucl. Phys. **A661**, 130c (1999).
- [17] M. Anderson *et al.*, Nucl. Instrum. Methods A **499**, 659 (2003); K. H. Ackerman *et al.* (STAR Collaboration), Nucl. Phys. **A661**, 681c (1999).
- [18] H. Wieman *et al.* (STAR Collaboration), IEEE Trans. Nucl. Sci. **44**, 671 (1997); W. Betts *et al.* (STAR Collaboration), *ibid.* **44**, 592 (1997); S. Klein *et al.* (STAR Collaboration), *ibid.* **43**, 1768 (1996).
- [19] C. Adler *et al.* (STAR Collaboration), Nucl. Instrum. Methods A **461**, 337 (2001).
- [20] J. Adams *et al.* (STAR Collaboration), Phys. Rev. C **71**, 044906 (2005).
- [21] C. Adler *et al.* (STAR Collaboration), Phys. Lett. **B595**, 143 (2004); S. Bekele, Ph.D. thesis, The Ohio State University, 2004 (<http://www.star.bnl.gov/central/publications/theses/2004>).
- [22] S. Eidelman *et al.*, Review of Particle Physics (PDG), Phys. Lett. **B592**, 1 (2004).
- [23] M. Gell-Mann and A. Pais, Phys. Rev. **97**, 1387 (1955).
- [24] V. L. Lyuboshitz and M. I. Podgoretsky, Sov. J. Nucl. Phys. **30**, 407 (1979).
- [25] G. Alexander and H. J. Lipkin, Phys. Lett. **B456**, 270 (1999).
- [26] G. Alexander, Rep. Prog. Phys. **66**, 481 (2003).
- [27] M. Gyulassy, Phys. Lett. **B286**, 211 (1992).
- [28] R. Lednicky and V. L. Lyuboshits, Sov. J. Nucl. Phys. **35**, 770 (1982).
- [29] B. Ananthanarayan, G. Colangelo, J. Gasser, and H. Leutwyler, Phys. Rep. **353**, 207 (2001).
- [30] J. Adams *et al.* (STAR Collaboration), Phys. Rev. Lett. **92**, 112301 (2004).
- [31] A. D. Martin, E. N. Ozmurtlu, and E. J. Squires, Nucl. Phys. **B121**, 514 (1977).
- [32] V. Baru *et al.*, Eur. Phys. J. A **23**, 523 (2005).
- [33] A. Antonelli (KLOE Collaboration), eConf C **020620**, THAT06 (2002).
- [34] N. N. Achasov and V. V. Gubin, Phys. Rev. D **63**, 094007 (2001); for f_0 , N. N. Achasov and A. N. Kiselev, *ibid.* **68**, 014006 (2003) for a_0 .
- [35] R. Lednicky, V. V. Lyuboshits, and V. L. Lyuboshits, Phys. At. Nucl. **61**, 2950 (1998).
- [36] J. Adams *et al.* (STAR Collaboration), accepted for publication; nucl-ex/0511003.
- [37] U. Heinz, Nucl. Phys. **A610**, 264 (1996).
- [38] J. Adams *et al.* (STAR Collaboration), Phys. Rev. Lett. **91**, 262301 (2003).
- [39] R. Lednicky, nucl-th/0501065.